

ARTICLE

Open Access

# A multiple myeloma-specific capture sequencing platform discovers novel translocations and frequent, risk-associated point mutations in *IGLL5*

Brian S. White<sup>1,5</sup>, Irena Lanc<sup>1</sup>, Julie O'Neal<sup>1</sup>, Harshath Gupta<sup>1</sup>, Robert S. Fulton<sup>2</sup>, Heather Schmidt<sup>2</sup>, Catrina Fronick<sup>2</sup>, Edward A. Belter Jr.<sup>2</sup>, Mark Fiala<sup>1</sup>, Justin King<sup>1</sup>, Greg J. Ahmann<sup>3</sup>, Mary DeRome<sup>4</sup>, Elaine R. Mardis<sup>2,6</sup>, Ravi Vijj<sup>1</sup>, John F. DiPersio<sup>1</sup>, Joan Levy<sup>4,8</sup>, Daniel Auclair<sup>4</sup> and Michael H. Tomasson<sup>1,7</sup>

## Abstract

Multiple myeloma (MM) is a disease of copy number variants (CNVs), chromosomal translocations, and single-nucleotide variants (SNVs). To enable integrative studies across these diverse mutation types, we developed a capture-based sequencing platform to detect their occurrence in 465 genes altered in MM and used it to sequence 95 primary tumor-normal pairs to a mean depth of 104x. We detected cases of hyperdiploidy (23%), deletions of 1p (8%), 6q (21%), 8p (17%), 14q (16%), 16q (22%), and 17p (4%), and amplification of 1q (19%). We also detected *IGH* and *MYC* translocations near expected frequencies and non-silent SNVs in *NRAS* (24%), *KRAS* (21%), *FAM46C* (17%), *TP53* (9%), *DIS3* (9%), and *BRAF* (3%). We discovered frequent mutations in *IGLL5* (18%) that were mutually exclusive of *RAS* mutations and associated with increased risk of disease progression ( $p = 0.03$ ), suggesting that *IGLL5* may be a stratifying biomarker. We identified novel *IGLL5/IGH* translocations in two samples. We subjected 15 of the pairs to ultra-deep sequencing (1259x) and found that although depth correlated with number of mutations detected ( $p = 0.001$ ), depth past ~300x added little. The platform provides cost-effective genomic analysis for research and may be useful in individualizing treatment decisions in clinical settings.

## Introduction

Multiple myeloma (MM) is a fatal malignancy of mature plasma B cells. Overt MM is preceded by a premalignant phase, monoclonal gammopathy of undetermined significance (MGUS), which can progress to smoldering MM and ultimately to fatal myeloma. Genetic alterations detected in premalignant MGUS cells are likely initiating events. These may be divided into two primary subtypes that are most often non-overlapping<sup>1</sup>: hyperdiploid (HRD)

myeloma is characterized by trisomies of most odd-numbered chromosomes<sup>2</sup>, while non-HRD myeloma frequently involves immunoglobulin heavy chain (*IGH*) translocations. These upregulate target oncogenes by placing them under the control of one or both of the powerful, B-cell-specific *IGH* enhancer regions; canonical *IGH* partner genes include *WHSC1/FGFR3*, *CCND3*, *CCND1*, *MAF*, and *MAFB* in translocations t(4;14), t(6;14), t(11;14), t(14;16), and t(14;20), respectively<sup>1</sup>. Secondary genetic events are detected in MM, but not its precursor phases, and are thought to drive disease progression. The most prevalent secondary events include *MYC* translocations (juxtaposing *IGH* and other loci), single-nucleotide variants (SNVs) involving *KRAS*, *NRAS*,

Correspondence: Michael H. Tomasson ([michael-tomasson@uiowa.edu](mailto:michael-tomasson@uiowa.edu))

<sup>1</sup>Department of Medicine, Washington University School of Medicine, St. Louis 63110 MO, USA

<sup>2</sup>McDonnell Genome Institute, Washington University School of Medicine, St. Louis 63108 MO, USA

Full list of author information is available at the end of the article

These authors contributed equally: Brian S. White, Irena Lanc.

© The Author(s) 2018



**Open Access** This article is licensed under a Creative Commons Attribution 4.0 International License, which permits use, sharing, adaptation, distribution and reproduction in any medium or format, as long as you give appropriate credit to the original author(s) and the source, provide a link to the Creative Commons license, and indicate if changes were made. The images or other third party material in this article are included in the article's Creative Commons license, unless indicated otherwise in a credit line to the material. If material is not included in the article's Creative Commons license and your intended use is not permitted by statutory regulation or exceeds the permitted use, you will need to obtain permission directly from the copyright holder. To view a copy of this license, visit <http://creativecommons.org/licenses/by/4.0/>.

and *DIS3*, and copy number variants (CNVs) that amplify chromosome arm 1q or delete 1p, 6q, 13, 14q, or 16q<sup>2</sup>.

This diversity of genetic lesions has recently been leveraged in a prognostic model that integrates the International Staging System (ISS)<sup>3</sup> with incidence of CNVs, SNVs, and translocations<sup>4</sup>. This ISS-MUT model increases precision over ISS alone in detecting early mortality and progression. Other studies have highlighted the context-dependent prognostic significance of variants across the spectrum of mutation types<sup>1</sup>. For example, trisomies of chromosomes 3 or 5 have been found to abrogate the poor overall survival associated with t(4;14) translocations<sup>5</sup>. Collectively, these results highlight the prognostic impact of the interplay between CNVs, SNVs, and translocations—the potential for co-occurring mutations to mitigate an otherwise poor outcome implies that testing a patient for all three types of mutations may help target chemotherapy regimens more accurately to specific patient subgroups in the future<sup>2</sup>.

Detecting myeloma-relevant mutations may be done via exome sequencing, as in the ISS-MUT study<sup>4</sup>. However, approaches targeting a subset of disease-associated genes should reduce computational analysis, facilitate quicker return of clinical results, and enable deeper sequencing at a fixed budget<sup>6</sup>. Indeed, targeted, clinical sequencing is performed with increasing frequency both commercially<sup>7</sup> and through cancer centers<sup>8–10</sup>. In the specific context of MM, an amplicon-based, 77-gene panel detects both CNVs and SNVs<sup>11</sup>. This extends an earlier panel<sup>6</sup> used to track mutation evolution across 47 genes<sup>12</sup>. Other efforts have focused on *IGH* rearrangements and translocations: amplicon-based sequencing of the locus effectively detects minimal residual disease<sup>13</sup>, while capture-based approaches have been used to discover *IGH* and *MYC* translocations<sup>14,15</sup>.

Similar enrichment technologies could be used to simultaneously detect CNVs, SNVs, and translocations. Indeed, one such platform was recently described—the approach involved targeted sequencing of the *IGH* locus and 246 genes implicated in MM and/or other cancers<sup>16</sup>. The platform was used to profile 14 MM cell lines and five primary samples. Maturing such approaches will require extensive validation and tuning of the associated bioinformatics methods. Towards this end, we developed a related MM-specific targeted sequencing platform and validated it against 95 primary tumor samples, 44 of which were previously subjected to exome sequencing and 22 of which were previously assayed by fluorescence in situ hybridization (FISH). We demonstrate high concordance of the platform with these exome sequencing and FISH results. Additionally, we describe novel approaches to tuning computational CNV and translocation calling methods. These optimized methods facilitated integrative analysis across mutation types, which

revealed patterns of mutual exclusivity and co-occurrence involving CNVs, SNVs, and translocations. We discovered novel translocations juxtaposing *IgLL5* with *IGH* and detected high-frequency mutations in *IgLL5*. These *IgLL5* mutations were mutually exclusive of *RAS* mutations and associated with disease progression, suggesting that *IgLL5* may be involved in disease pathogenesis and/or serve as a biomarker of high-risk MM.

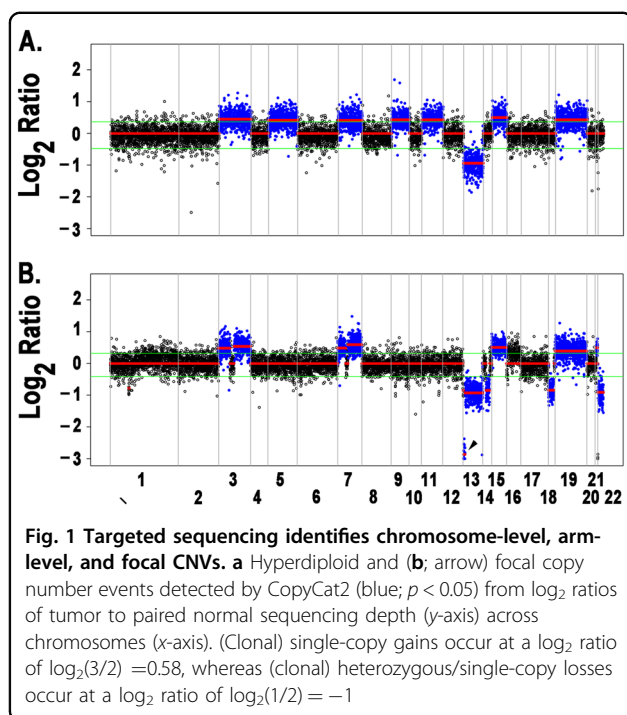
## Methods

We designed a Nimblegen probe set (Roche) targeting 3.3 Mb of space that includes 465 genes and the *IGH* region. Sequencing library pools were prepared, hybridized to the probes, and sequenced on the HiSeq2000 (2 × 100 reads for initial sequencing of 95 tumor-normal pairs) or the HiSeq2500 (2 × 125 reads for deep sequencing of a subset of 15 pairs). Reads were aligned against human reference genome GRCh37-lite using BWA<sup>17</sup>. Acquired SNVs were called in each tumor sample relative to its paired normal sample using samtools<sup>18</sup>, SomaticSniper<sup>19</sup>, MuTect<sup>20</sup>, Strelka<sup>21</sup>, and VarScan2 (ref. <sup>22</sup>). Translocations were called using LUMPY<sup>23</sup>, with results filtered by a machine learning approach optimized to achieve high precision relative to available FISH results. CNVs were called using CopyCAT2 (<https://github.com/abelhj/cc2/>; ref. <sup>24</sup>) parameterized to detect copy number alterations exceeding the level of noise estimated from diploid regions using a gaussian mixture model (<https://github.com/genome/bmm>). Additional information is provided in Supplementary Methods.

## Results

We developed a MM-specific custom capture sequencing platform capable of detecting CNVs, SNVs, and translocations. We designed oligonucleotide probes covering 3.3 Mb of genomic space and complementary to the exons, untranslated regions, and splice sites of 465 genes (Tables S1 and S2) expressed in MM that: (1) are annotated as cancer genes (in COSMIC<sup>25</sup> or MutSig<sup>26</sup>), (2) function in DNA repair or B-cell biology, (3) are mutated at a frequency of >3% in published studies<sup>27,28</sup>, or (4) have mutations that cluster in hotspots. To detect *IGH* translocations, we also designed probes tiled in an unbiased manner across the locus, including within the variable (*IGHV*), diversity (*IGHD*), joining (*IGHJ*), and constant/switch regions. We also designed probes targeting the exonic regions of canonical *IGH* translocation partners (*CCND1*, *CCND3*, *FGFR3*, *MAF*, *MAFB*, *WHSC1*, and *WWOX*). To capture secondary *MYC* translocations, we tiled probes across exonic and intronic regions of the *MYC* locus.

We used the platform to sequence DNA isolated from 95 tumor (CD138-purified cells isolated from bone marrow aspirates) and paired normal (blood) samples. These



samples were specifically selected to validate our platform and to tune our computational methods as a subset of them were previously subjected to exome sequencing (44 samples) and/or FISH (22 samples) analysis of *IGH* translocations. We achieved a mean sequencing depth of 104 $\times$  (min = 33 $\times$ , max = 140 $\times$ ; Supplementary Figure S1A) across the tumor samples and of 107 $\times$  (min = 43 $\times$ , max = 168 $\times$ ; Supplementary Figure S1B) across the normal samples.

#### Targeted capture sequencing identifies copy number alterations with prognostic significance

The broad coverage of the platform [across chromosome arms (Table S3) and 465 genes] facilitated detection of chromosome-level, arm-level, and focal CNVs. We identified these events computationally from the per-probe ratios of tumor to normal sequencing depth using CopyCAT2 (ref.<sup>24</sup>). To reduce false positives, we developed an approach that filtered CNV calls with ratios below a noise level estimated from diploid regions (Supplementary Figure S2A–C). Our approach identified the full range of CNVs, from genome-scale hyperdiploid events (Fig. 1a; Table S4) to focal events, including a homozygous deletion that encompassed *BRCA2* (Fig. 1b). Detected arm-level events included those associated with poor prognosis such as amp(1q), del(1p), del(13q), and del(17p) (reviewed in ref.<sup>1</sup>; Supplementary Figure S2D).

#### Targeted capture sequencing identifies *IGH* translocations

We detected *IGH* translocations using LUMPY and again developed a filtering strategy to reduce likely false

**Table 1 Frequency of Translocations**

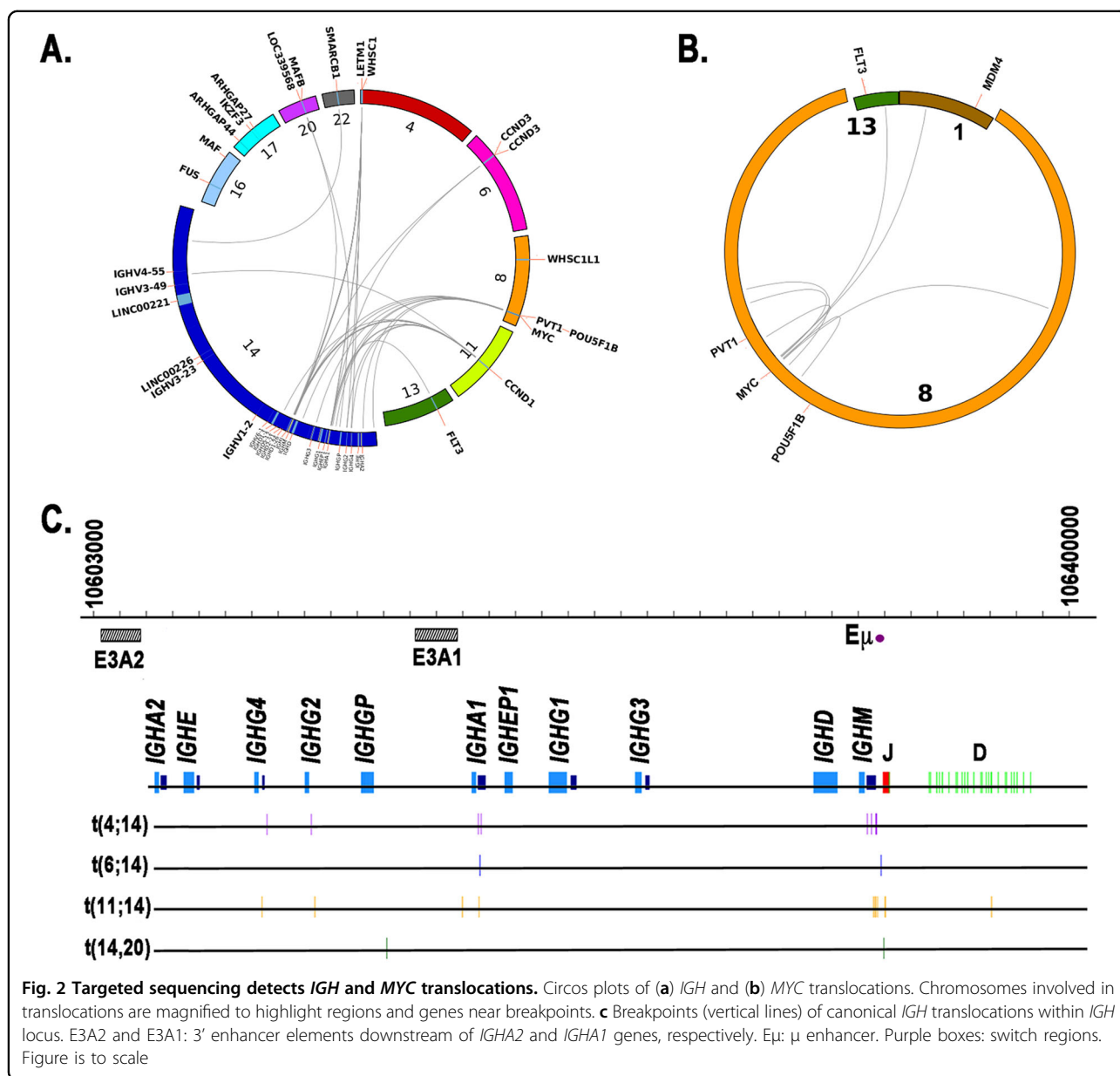
Translocation	Frequency (%)
t(11;14)	14
t(4;14)	13
t(8;14)	7
t(6;14)	2
t(14;20)	2

positives. We filtered putative translocations based on thresholds on the number of supporting split reads and discordant paired-end reads. We tuned the thresholds to maximize precision using a machine learning approach and available FISH data, resulting in a precision of 100% and a recall of 64% (Supplementary Figure S3; Supplementary Table S5). Canonical *IGH* translocations were then detected by the platform near expected frequencies (Table 1; Fig. 2a) and occurred predominantly within the *IGH* constant region, but also telomeric of the *IGHM* switch region and occasionally within the D and J regions (Fig. 2c). Notably, one of the t(11;14) translocations occurred within the constant region, but outside all constant and switch segments. These results are consistent with a recent study<sup>15</sup>, which found *IGH* translocations occurring within each of these regions. No translocations within the V region passed the filtering step.

#### *IGLL5* is translocated and co-incident with overexpression of *DERL3* in multiple myeloma

To prioritize novel *IGH* translocations as potential driver mutations, we identified cancer-associated genes within 1 Mb of each chromosomal breakpoint (Supplementary Table S6). The two annotated translocations with largest total evidence (sum of number of supporting split reads and number of discordant paired-end reads) were analyzed further. The first was a complex translocation involving chromosomes 11, 13, and 14. The putative breakpoint on chromosome 13 was nearby *FLT3* (<0.5 Mb; Supplementary Figure S4); we validated that chromosome 13q12.2 was indeed translocated to *IGH* on chromosome 14 using PCR.

Breakpoints of the second highly-supported translocation, t(14;22)(q32.33;q11.22), were located within *IGH* and *IGLL5*, which is spanned by the immunoglobulin lambda light chain locus (Fig. 3a). To validate this translocation, we performed PCR amplification of the putative breakpoint on DNA isolated from the patient in which it was detected. A PCR product of the expected size was detected in CD138<sup>+</sup> tumor cells but not in the peripheral blood mononuclear control [Fig. 3b (top)]. Re-sequencing



and mapping of the tumor-specific PCR product confirmed the reciprocal translocation spanned chromosomes 14 and 22. Small regions were deleted on both derivative chromosomes and thus could be used to selectively amplify the corresponding wild-type (WT) chromosomes. We designed primers within these deleted regions and used them to perform PCR amplification, which confirmed the retention of one copy of each of the WT chromosomes in the tumor sample [Fig. 3b (bottom)].

To search for additional *IGLL5* translocations, we relaxed our filtering constraints and found a second sample predicted by LUMPY to harbor a t(14;22) translocation, though no DNA was available for validation. The validated t(14;22) translocation was predicted to juxtapose

the  $\mu$  and 3' enhancers (chr14:106032614–106167601) with *DERL3*. Hence, we looked for evidence of overexpression of *DERL3* and other cancer-associated genes within 1 Mb of the predicted breakpoint on chromosome 22 (*IGLL5*, *BCR*, and *SMARCB1*) by examining RNA-seq expression data from a partially overlapping set of 84 MM patients. We found outlying expression of *DERL3* in six of these samples (exceeding 1.5 $\times$  the FPKM interquartile range), including the second sample with a putative t(14;22) translocation (Fig. 3c; no expression data were available for the sample harboring the validated translocation). Additionally, we found that *DERL3* was overexpressed in MM relative to other cancer types within the Cancer Cell Line Encyclopedia (CCLE)<sup>29</sup> (Supplementary

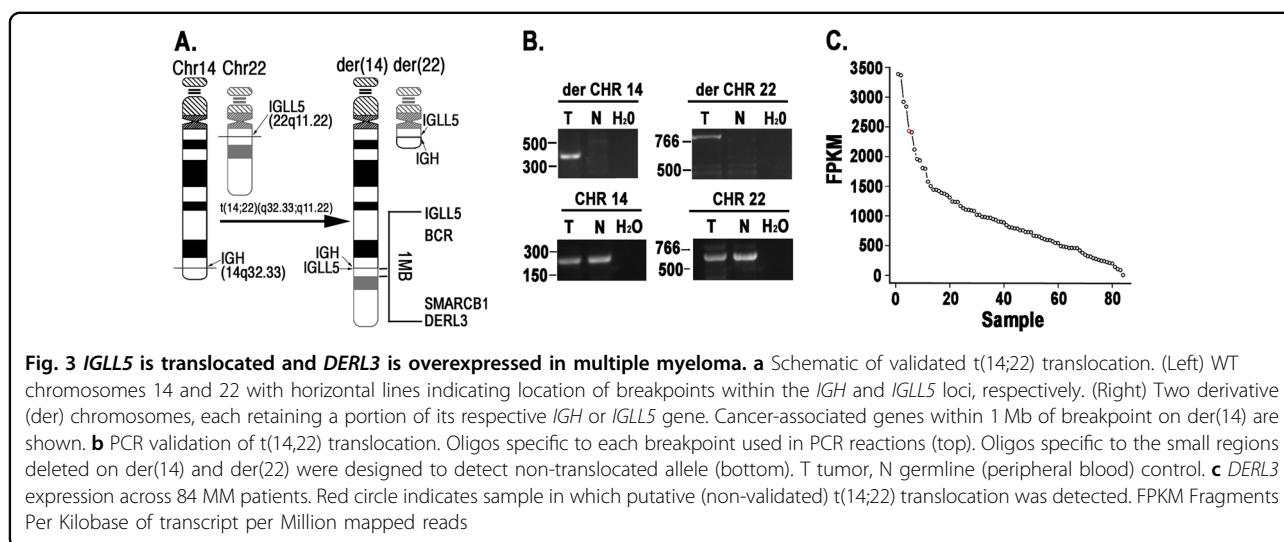


Figure S5), with high expression also reported in other B-cell malignancies. We also examined expression of *IGLL5* both within our cohort and CCLE. *IGLL5* expression was in the 82nd percentile in the putatively translocated sample for which we had RNA-seq data, though it is not noticeably elevated with respect to the mean expression (data not shown). *IGLL5* expression in MM cell lines within the CCLE is second only to Burkitt's Lymphoma cell lines; more generally, and as with *DERL3*, *IGLL5* expression is higher in B-cell malignancies than in other cancer types. Taken together, these data suggest that *DERL3* may be dysregulated in MM via *IGH* translocation or another unknown mechanism.

#### Targeted capture sequencing identifies intra- and inter-chromosomal *MYC* translocations

FISH validation data of *MYC* translocations were not available to tune LUMPY parameters and, as a result, intra- and (non-*IGH*) inter-chromosomal *MYC* translocations were called at a high false-positive rate (in every tumor and normal sample, Supplementary Figure S6). To accurately detect somatic *MYC* translocations, we developed a machine learning-based approach tuned to filter putative *MYC* translocations called in normal samples. Applying this method to tumor samples resulted in five intra-chromosomal and two non-*IGH* inter-chromosomal *MYC* translocations, with one sample having one intra- and one inter-chromosomal translocation (6 of 95, 6%, Fig. 2b; Supplementary Table S7). The intra-chromosomal translocations involved neighboring genes *PVT1* and *POU5F1B*, as previously reported<sup>14</sup>.

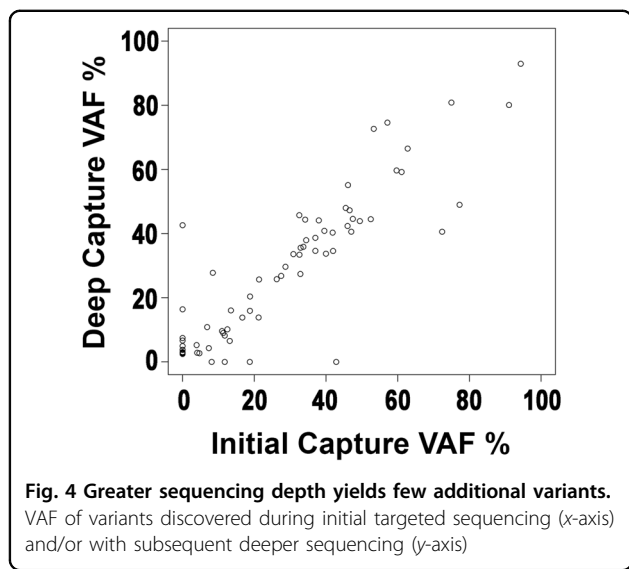
#### Targeted capture sequencing identifies non-silent single-nucleotide variants in all tumor samples

All tumor samples harbored at least one somatic (missense, nonsense, or frame-shift) mutation, with each

sample having a mean of 20 mutations (Supplementary Table S8). A total of 443 genes had a non-synonymous (frame-shift insertion or deletion, missense, or nonsense) mutation in one or more samples; 581 genes had a mutation of any kind in one or more samples. Ninety-four of 95 tumor samples had a mutation predicted to be deleterious by Poly-Phen2<sup>30</sup> or SIFT<sup>31</sup>, with each sample having a mean of twelve deleterious mutations. In 24 instances, we observed a gene harboring multiple mutations previously associated with cancer (via COSMIC). This occurred in thirteen samples across seventeen genes, including *KRAS* and *RBI*; both were among the most frequently observed (in three samples).

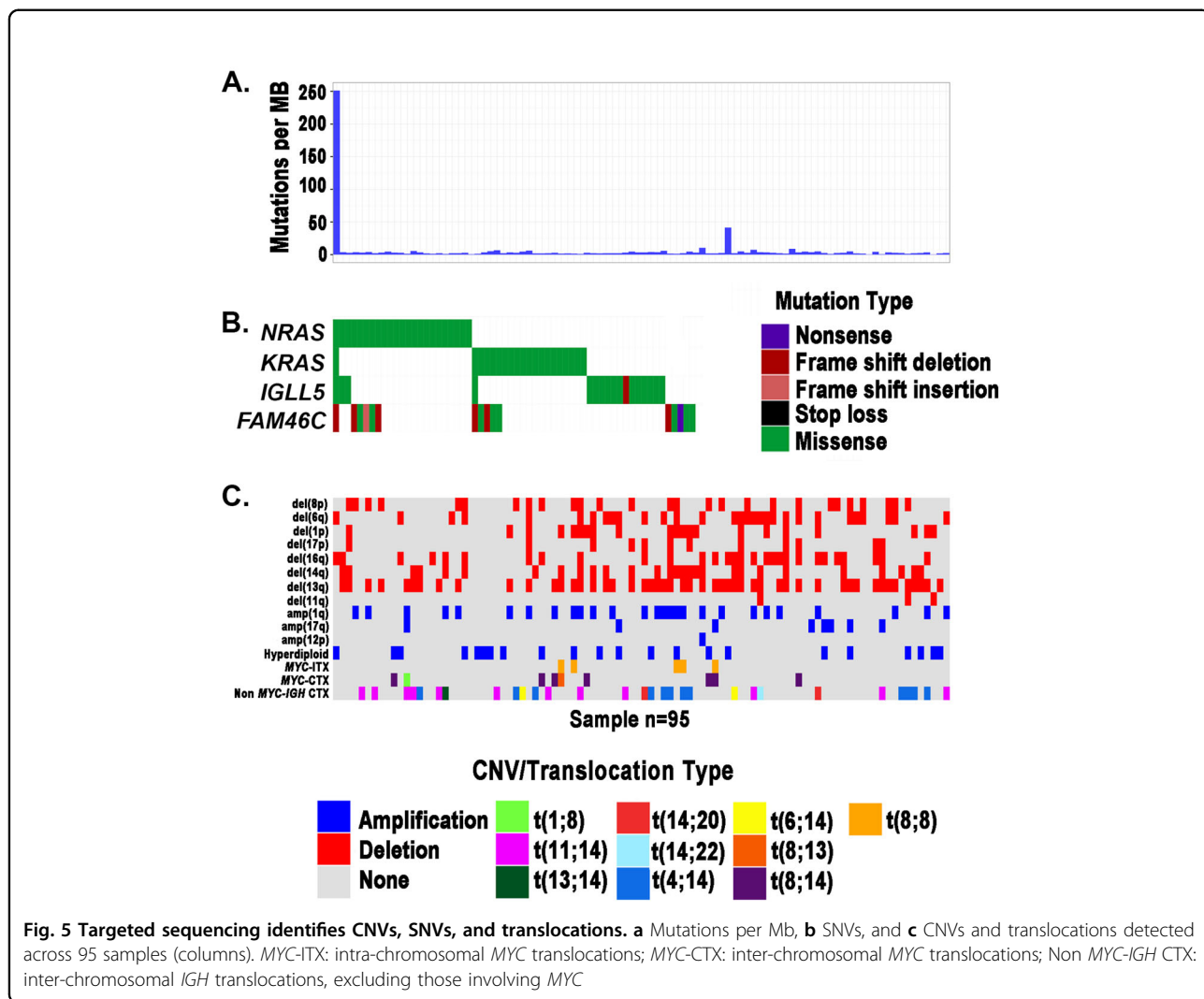
#### Increased sequencing depth yields few additional variants

To determine whether MM is characterized by deeply subclonal variants of biological significance, we performed additional sequencing of 15 tumor (mean depth = 1,259 $\times$ , min = 506 $\times$ , max = 1,660 $\times$ ) and paired normal (mean = 1,326 $\times$ , min = 763 $\times$ , max = 1,727 $\times$ ) samples. We then compared the allele frequencies of variants discovered during the original and/or subsequent deep sequencing (Fig. 4). To focus on high-confidence events likely to be of biological relevance, we removed silent variants, those in intronic, intergenic, or flanking regions, those in *IGH* (and, hence, likely arising due to somatic hypermutation), or those that were flagged as likely germline variants by at least one caller in at least one study. This resulted in 57 variants in the original sequencing study (mean depth = 92 $\times$ ) and 67 variants in the subsequent study (mean depth = 1,169 $\times$ ). Variant allele frequencies (VAFs) of mutations shared across the two studies were highly correlated ( $R^2 = 0.80$ ;  $p < 2.2e-16$ ). As expected, the vast majority of variants unique to either study had low VAFs: one of the four variants unique to the original study had a VAF <10%, though all had an alternate allele count of



three or fewer supporting reads, while 12 of the 14 variants unique to the subsequent study had a VAF <10%. Though relatively few new variants were discovered by the additional sequencing, these did include several annotated in COSMIC in genes *KRAS*, *HECW1*, and *ZFHX4*.

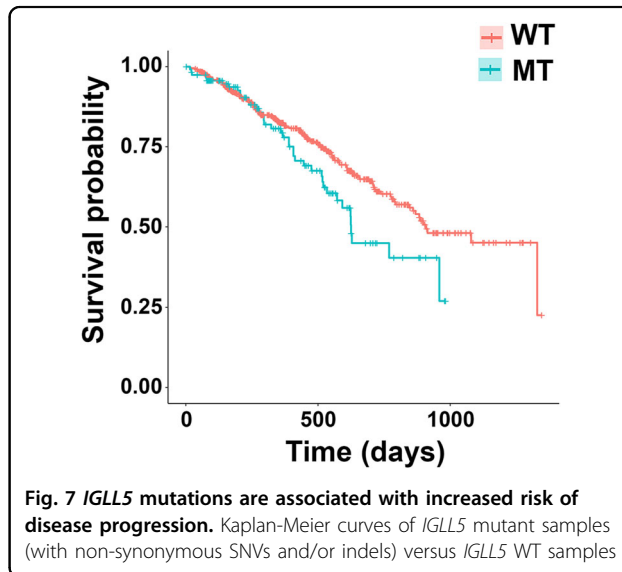
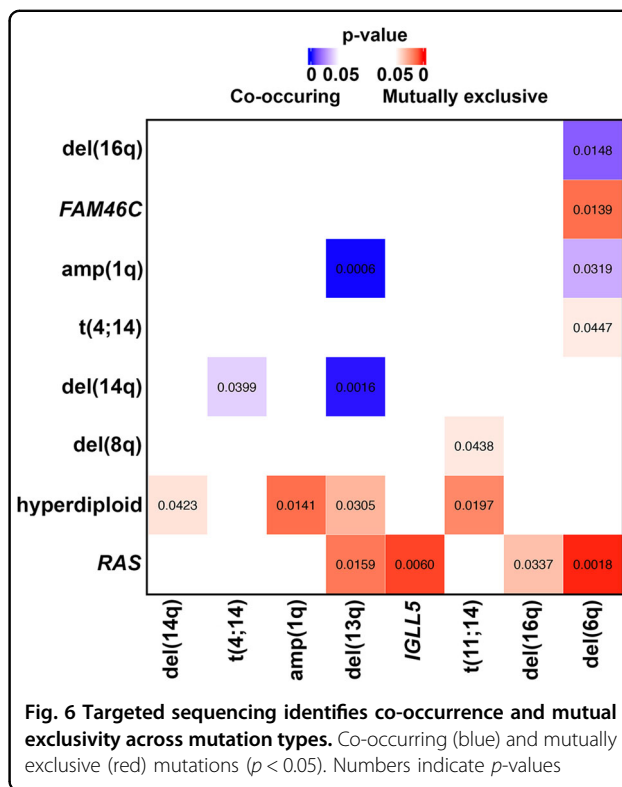
These results were recapitulated in a comparison of the variants discovered in 44 samples subjected to capture-based sequencing (mean depth of 1,562 capture-based variants = 123x) and previously to exome sequencing (mean depth of 3,563 exome variants = 136x; Supplementary Figure S7). As in our above comparison, the 1,450 mutations discovered in both studies had highly correlated VAFs ( $R^2 = 0.85$ ;  $p < 2.2e-16$ ). Again, the majority of variants unique to one study had low VAF: 79 of 112 variants unique to the capture-based study (Supplementary Fig. S7C) and 2,066 of the 2,113 variants unique to the exome-based study (Supplementary Figure S7B) had VAFs <10%.



To further explore the effects of sequencing depth, we downsampled the sequencing reads from the 15 deeply-sequenced samples, called variants on the downsampled reads, and plotted the total number of variants following filtering (as above) in the downsampled and full data set (Supplementary Figure S8). As expected, the number of variants was correlated with sequencing depth ( $R^2 = 0.52$ ;  $p = 10^{-3}$ ). However, beyond  $\sim 25\%$  of the final sequencing depth (or a mean depth of  $\sim 300\times$ ), the increase in number of discovered variants is marginal. Similar performance was observed at an even lower depth of  $92\times$  in the aforementioned case of the 15 original capture results later re-sequenced. Together, these results indicate that depths as low as  $100\times$  can capture the majority of variants of interest and that coverage beyond  $300\times$  will lead to sharply diminishing returns.

#### Targeted capture sequencing facilitates integrative analysis across mutation types

Integrated analysis of CNVs, SNVs, and translocations highlights patterns of mutual exclusivity and co-occurrence both within and across mutation types (Fig. 5). We tested for significance of these patterns after excluding the apparent hypermutator sample (leftmost column; Fig. 5a) to improve statistical power. This revealed mutation co-occurrence (blue; Fig. 6; Table S9) within CNVs [i.e., of del(6q) with del(16q) and amp(1q) and of del(13q) with amp(1q) and del(14q)] and involving CNVs and translocations [i.e., of del(14q) with t(4;14)]. As expected, we detected mutual exclusivity (red; Fig. 6; Table S9) between hyperdiploidy and t(11;14). We also detected cross-mutation type exclusivity between CNVs and SNVs [i.e., both *RAS* mutations (i.e., *KRAS* or *NRAS*) and *FAM46C* are mutually exclusive with del(6q)]. *IGLL5* was the third most frequently mutated gene in our data set (Fig. 5b; 18%), with (silent and non-synonymous) *IGLL5* mutations enriched for a c-AID signature (i.e., C to T/G mutation at WRCY motifs;  $p = 2.7 \times 10^{-6}$ ; binomial test). Thirty-eight of the 40 detected *IGLL5* SNVs occurred in amino acid positions one to 100, outside of any annotated protein domains. The remaining two (K166N and K189R) occurred in the immunoglobulin C1-set domain. Mutations in *IGLL5* were mutually exclusive of *RAS* mutations ( $p = 0.006$ ), with trends toward mutual exclusivity with *KRAS* ( $p = 0.054$ ), *NRAS* ( $p = 0.111$ ), and *FAM46C* ( $p = 0.113$ ), independently (Figs 5 and 6). *IGLL5* mutations in diploid loci had a median VAF of 58% and a first quartile VAF of 39%, suggesting that the majority are likely clonal (Supplementary Figure S9). Finally, we found that *IGLL5* SNVs are associated with disease progression [Fig. 7; hazard ratio = 1.46 (95% confidence interval: 1.03–2.08);  $p = 0.03$  (log-rank test)].



#### Discussion

We developed a MM-specific, capture-based sequencing platform targeting 465 genes that detects CNVs, SNVs, and translocations. We used the platform to sequence 95 tumor/normal pairs and validated its ability to detect SNVs and translocations using exome sequencing and FISH data. After developing custom computational approaches for reducing false positives, we detected

CNVs (Fig. 1) and known *IGH* translocations at expected frequencies (Fig. 2; Table 1) and discovered rare novel chromosomal translocations (Fig. 3). By deeply sequencing 15 pairs, we showed that there is a marginal increase in number of non-silent variants discovered with sequencing depth (Fig. 4). Hence, many scientific and some clinical goals may be achievable with the more modest sequencing depth (~100×) used for the complete cohort of 95 pairs.

We detected (intra- and inter-chromosomal) *MYC* translocations at a frequency of 13% [95% CI (7%-20%); 12 of 95; Fig. 2; Tables S5 and S7]. This is generally consistent with prior studies, though a considerable range of frequencies has been published. Such discrepancies are likely due in part to differences in sample size, disease stage, assay, and assay optimization/tuning. An early study using FISH reported complex *MYC* abnormalities in 50% of primary tumors—however, the analyzed samples were few [7 of 14; 95% CI (26%-74%)] and advanced (stage III)<sup>32</sup>. *MYC* translocation frequencies more similar to those we observed have been detected in newly diagnosed MM patients using both FISH—15% [79 of 529; 95% CI (12%-18%)]<sup>33</sup> and 23% [62 of 274; 95% CI (18%-28%)]<sup>34,35</sup>—and a capture-based next-generation sequencing approach similar to that presented here—20% [21 of 104; 95% CI (13%-28%)]<sup>14</sup>.

Our data revealed that *IGLL5* is mutated via both point substitutions and translocations in MM (Figs 2, 3 and 5). The SNVs within the locus likely result from somatic hypermutation of the immunoglobulin lambda light chain locus, which spans *IGLL5*. Indeed, we saw an enrichment for AID-induced mutations within *IGLL5*, as has been previously observed in chronic lymphocytic leukemia (CLL), where the gene is frequently mutated<sup>36</sup>. We found that non-synonymous *IGLL5* mutations are both mutually exclusive with *RAS* mutations (Fig. 6) and associated with disease progression (Fig. 7) and, with a median VAF of 58%, are likely present in the founding clone. Together, these findings suggest that *IGLL5* mutation may contribute to myeloma pathogenesis, but without additional data their functional significance remains unknown. The fact that mutations and translocations do not recurrently affect specific residues in the *IGLL5* protein supports a loss of function model, but an alternative hypothesis is that *IGLL5* mutations are simply a biomarker for high-risk disease.

We observed that *IGLL5* was translocated to the *IGH* locus in two patient samples (Figs. 2 and 3). Translocations between *IGH* and either of the two light chain loci have been reported in B cells and their associated disorders: *IGL/IGH* translocations have been reported in non-Hodgkin lymphoma<sup>37</sup> and in activated B cells<sup>38</sup> where it was suggested that the translocations resulted from deficiencies in non-homologous end-joining that

induced both V(D)J-recombination-associated breaks at the *IGL* locus and class switch recombination-associated *IGH* breaks. The authors speculated that, since the translocations conferred no obvious selective advantage, these translocations simply reflected the mechanistic opportunity presented by two frequently-broken and spatially-proximal loci<sup>38</sup>. *IGH* translocations partnered instead with *IGK* have been detected in B-cell lymphomas<sup>39</sup> and in a patient-derived B lymphoblastoid cell line<sup>40</sup> with the latter plausibly attributable to the patient's prior, long-term treatment with a DNA-damaging alkylating agent. The possibility remains that the translocations we detected play a functional role by co-opting a large super-enhancer downstream of *IGLL5*, which was found to be active within the MM1.S MM cell line<sup>41</sup>. Its position between *IGLL5* and *BCR* place it on the der(14) chromosome of the t(14;22) translocation we validated. Hence, this super-enhancer may amplify the effect of the *IGH* enhancers in upregulating the expression of nearby genes translocated to chromosome 14. Indeed, we observed upregulation of one such gene, *DERL3*, across MM tumors relative to other cancer types, generally (Supplementary Figure S5), and in the sample with the second putative t(14;22) translocation, specifically (Fig. 3). Overexpression of *DERL3* could play a role in MM by increasing endoplasmic reticulum (ER)-associated degradation within the proteasome. *DERL3* forms an export channel in the ER through which misfolded proteins fated for degradation reach the proteasome<sup>42</sup>. The proteasome inhibitor bortezomib is highly efficacious in MM cells. Hence, were it to instead promote, rather than inhibit, activity of the proteasome, *DERL3* overexpression might confer a selective advantage to MM cells. Future experiments are required to decipher the importance of *IGLL5* translocations and the significance of *DERL3* overexpression.

In addition to detecting known mutations, the platform was designed to enable discovery: (1) We queried 465 genes, a much larger set than assayed by previous targeted platforms<sup>6,11,16</sup>, and (2) we tiled across the entire V, D, and J regions, as opposed to restricting probes to annotated segments within these regions<sup>15</sup> in an attempt to detect translocations involving inter-segment regions of the locus. Additional experience will be necessary to evaluate these design decisions. For example, lack of inferred translocations involving the J region may suggest that probes used to tile across this ~700 Kb region are better invested elsewhere. In particular, future versions of the platform should provide currently lacking coverage of chromosome arm Yq, though the tandem-rich arms of acrocentric chromosomes (13p, 14p, 15p, 22p, and Yp) will remain difficult to capture. Additionally, targeting probes to common SNPs would enable detection of allele-specific ploidy at



a given locus<sup>43</sup>, which would facilitate SNV-based inference of clonal evolution<sup>44</sup>.

Mutation<sup>4</sup> and expression<sup>45</sup> data, coupled with ISS stage, have been shown to improve prognostic accuracy over ISS stage alone. Indeed, two recent crowd-sourcing competitions [a DREAM challenge (<https://www.synapse.org/#!/Synapse:syn6187098/wiki/401884>; refs<sup>46,47</sup> and a Topcoder challenge ([http://crowdsourcing.topcoder.com/myeloma\\_predictor](http://crowdsourcing.topcoder.com/myeloma_predictor))] aim to improve MM patient stratification using genomic, transcriptomic/expression, cytogenetic, and clinical features. The ease of employing a single platform to assay CNVs, SNVs, and translocations would facilitate these and related efforts. Significantly, the same probes could be used to perform targeted RNA sequencing, which would also furnish these studies with comparative gene expression across samples.

#### Author contribution

B.S.W., I.L., J.O., H.G., and M.H.T. designed the experiments, performed research and wrote the manuscript; C.F., E.A.B., M.F., G.J.A., M.D., and J.K. performed research; R.S.F. and H.S. designed the experiments and performed research; E.R. M., R.V., J.F.D., and J.L. designed the experiments; D.A. designed the experiments and wrote the manuscript.

#### Author details

<sup>1</sup>Department of Medicine, Washington University School of Medicine, St. Louis 63110 MO, USA. <sup>2</sup>McDonnell Genome Institute, Washington University School of Medicine, St. Louis 63108 MO, USA. <sup>3</sup>Division of Hematology-Oncology, Mayo Clinic, Rochester 55905 MN, USA. <sup>4</sup>Multiple Myeloma Research Foundation, Norwalk, CT 06851, USA. <sup>5</sup>Present address: Sage Bionetworks, Seattle, WA 98109, USA. <sup>6</sup>Present address: Genomics Institute, Nationwide Children's Hospital, Columbus, OH 43205, USA. <sup>7</sup>Present address: Division of Hematology, Oncology and Bone Marrow Transplantation, 5204 MERF, University of Iowa, Iowa City, IA 52242, USA. <sup>8</sup>Present address: Chordoma Foundation, Durham, NC 27702, USA

#### Conflict of interest

The authors declare that they have no conflict of interest.

#### Publisher's note

Springer Nature remains neutral with regard to jurisdictional claims in published maps and institutional affiliations.

**Supplementary Information** accompanies this paper at (<https://doi.org/10.1038/s41408-018-0062-y>).

Received: 21 July 2017 Revised: 10 December 2017 Accepted: 18 December 2017

Published online: 21 March 2018

#### References

- Manier, S. et al. Genomic complexity of multiple myeloma and its clinical implications. *Nat. Rev. Clin. Oncol.* **14**, 100–103 (2016).
- Morgan, G. J., Walker, B. A. & Davies, F. E. The genetic architecture of multiple myeloma. *Nat. Rev. Cancer* **12**, 335–348 (2012).
- Greipp, P. R. et al. International staging system for multiple myeloma. *J. Clin. Oncol.* **23**, 3412–3420 (2005).
- Walker, B. A. et al. Mutational spectrum, copy number changes, and outcome: results of a sequencing study of patients with newly diagnosed myeloma. *J. Clin. Oncol.* **33**, 3911–3920 (2015).
- Chretien, M. L. et al. Understanding the role of hyperdiploidy in myeloma prognosis: which trisomies really matter? *Blood* **126**, 2713–2719 (2015).
- Kortum, K. M. et al. Targeted sequencing using a 47 gene multiple myeloma mutation panel (M(3) P) in -17p high risk disease. *Br. J. Haematol.* **168**, 507–510 (2015).
- Frampton, G. M. et al. Development and validation of a clinical cancer genomic profiling test based on massively parallel DNA sequencing. *Nat. Biotechnol.* **31**, 1023–1031 (2013).
- Cheng, D. T. et al. Memorial Sloan Kettering-integrated mutation profiling of actionable cancer targets (MSK-IMPACT): a hybridization capture-based next-generation sequencing clinical assay for solid tumor molecular oncology. *J. Mol. Diagn.* **17**, 251–264 (2015).
- Cottrell, C. E. et al. Validation of a next-generation sequencing assay for clinical molecular oncology. *J. Mol. Diagn.* **16**, 89–105 (2014).
- Garofalo, A. et al. The impact of tumor profiling approaches and genomic data strategies for cancer precision medicine. *Genome Med.* **8**, 79 (2016).
- Kortum, K. M. et al. Panel sequencing for clinically oriented variant screening and copy number detection in 142 untreated multiple myeloma patients. *Blood Cancer J.* **6**, e397 (2016).
- Kortum, K. M. et al. Longitudinal analysis of 25 sequential sample-pairs using a custom multiple myeloma mutation sequencing panel (M(3)P). *Ann. Hematol.* **94**, 1205–1211 (2015).
- Martinez-Lopez, J. et al. Prognostic value of deep sequencing method for minimal residual disease detection in multiple myeloma. *Blood* **123**, 3073–3079 (2014).
- Walker, B. A. et al. Translocations at 8q24 juxtapose MYC with genes that harbor superenhancers resulting in overexpression and poor prognosis in myeloma patients. *Blood Cancer J.* **14**, 13 (2014).
- Walker, B. A. et al. Characterization of IGH locus breakpoints in multiple myeloma indicates a subset of translocations appear to occur in pregerminal center B cells. *Blood* **121**, 3413–3419 (2013).
- Bolli, N. et al. A DNA target-enrichment approach to detect mutations, copy number changes and immunoglobulin translocations in multiple myeloma. *Blood Cancer J.* **6**, e467 (2016).
- Li, H. & Durbin, R. Fast and accurate short read alignment with Burrows-Wheeler transform. *Bioinformatics* **25**, 1754–1760 (2009).
- Li, H. et al. The Sequence Alignment/Map format and SAMtools. *Bioinformatics* **25**, 2078–2079 (2009).
- Larson, D. E. et al. SomaticSniper: identification of somatic point mutations in whole-genome sequencing data. *Bioinformatics* **28**, 311–317 (2012).
- Cibulskis, K. et al. Sensitive detection of somatic point mutations in impure and heterogeneous cancer samples. *Nat. Biotechnol.* **31**, 213–219 (2013).
- Saunders, C. T. et al. Strelka: accurate somatic small-variant calling from sequenced tumor-normal sample pairs. *Bioinformatics* **28**, 1811–1817 (2012).
- Koboldt, D. C. et al. VarScan 2: somatic mutation and copy number alteration discovery in cancer by exome sequencing. *Genome Res.* **22**, 568–576 (2012).
- Layer, R. M., Chiang, C., Quinlan, A. R. & Hall, I. M. LUMPY: a probabilistic framework for structural variant discovery. *Genome Biol.* **15**, R84 (2014).
- Sehn, J. K., Abel, H. J. & Duncavage, E. J. Copy number variants in clinical next-generation sequencing data can define the relationship between simultaneous tumors in an individual patient. *Exp. Mol. Pathol.* **97**, 69–73 (2014).
- Forbes, S. A. et al. COSMIC: exploring the world's knowledge of somatic mutations in human cancer. *Nucleic Acids Res.* **43**, D805–D811 (2015).
- Lawrence, M. S. et al. Mutational heterogeneity in cancer and the search for new cancer-associated genes. *Nature* **499**, 214–218.
- Bolli, N. et al. Heterogeneity of genomic evolution and mutational profiles in multiple myeloma. *Nat. Commun.* **5**, 2997 (2014).
- Chapman, M. A. et al. Initial genome sequencing and analysis of multiple myeloma. *Nature* **471**, 467–472 (2011).
- Barretina, J. et al. The Cancer Cell Line Encyclopedia enables predictive modelling of anticancer drug sensitivity. *Nature* **483**, 603–607 (2012).
- Adzhubei, I. A. et al. A method and server for predicting damaging missense mutations. *Nat. Methods* **7**, 248–249 (2010).
- Kumar, P., Henikoff, S., Fau—Ng, P. C. & Ng, P. C. Predicting the effects of coding non-synonymous variants on protein function using the SIFT algorithm. *Nat. Protoc.* **4**, 1073–1081 (2009).
- Shou, Y. et al. Diverse karyotypic abnormalities of the c-myc locus associated with c-myc dysregulation and tumor progression in multiple myeloma. *Proc. Natl Acad. Sci. USA* **97**, 228–233 (2000).

33. Avet-Loiseau, H. et al. Rearrangements of the c-myc oncogene are present in 15% of primary human multiple myeloma tumors. *Blood* **98**, 3082–3086 (2001).
34. Weinhold, N. et al. Concomitant gain of 1q21 and MYC translocation define a poor prognostic subgroup of hyperdiploid multiple myeloma. *Haematologica* **101**, e116–e119 (2016).
35. Neben, K. et al. Administration of bortezomib before and after autologous stem cell transplantation improves outcome in multiple myeloma patients with deletion 17p. *Blood* **119**, 940–948 (2012).
36. Kasar, S. et al. Whole-genome sequencing reveals activation-induced cytidine deaminase signatures during indolent chronic lymphocytic leukaemia evolution. *Nat. Commun.* **6**, 8866 (2015).
37. Aamot, H. V., Bjornslett, M., Delabie, J. & Heim, S. t(14;22)(q32; q11) in non-Hodgkin lymphoma and myeloid leukaemia: molecular cytogenetic investigations. *Br. J. Haematol.* **130**, 845–851 (2005).
38. Wang, J. H. et al. Mechanisms promoting translocations in editing and switching peripheral B cells. *Nature* **460**, 231–236 (2009).
39. Subramaniam, S., Geyer, J. T., Liu, Y. C. & Mathew, S. A translocation t(2;14)(p11.2; q32) involving rearrangements of immunoglobulin heavy chain and kappa light chain genes in B-cell lymphoma. *Leuk. Lymphoma* **56**, 2992–2994 (2015).
40. Kennedy, M. A. Novel chromosome translocation caused by fusion of immunoglobulin heavy and light chain V genes in a human B lymphoblastoid cell line. *J. Exp. Med.* **173**, 1033–1036 (1991).
41. Loven, J. et al. Selective inhibition of tumor oncogenes by disruption of super-enhancers. *Cell* **153**, 320–334 (2013).
42. Oda, Y. et al. Derlin-2 and Derlin-3 are regulated by the mammalian unfolded protein response and are required for ER-associated degradation. *J. Cell. Biol.* **172**, 383–393 (2006).
43. Van Loo, P. et al. Allele-specific copy number analysis of tumors. *Proc. Natl Acad. Sci. USA* **107**, 16910–16915 (2010).
44. Roth, A. et al. PyClone: statistical inference of clonal population structure in cancer. *Nat. Methods* **11**, 396–398 (2014).
45. Kuiper, R. et al. Prediction of high- and low-risk multiple myeloma based on gene expression and the International Staging System. *Blood* **126**, 1996–2004 (2015).
46. Mason, N. et al. Multiple Myeloma DREAM Challenge: A crowd-sourced challenge to improve identification of high-risk patients. *Cancer Research* **77**, 4725–4725 (2017).
47. Dervan, A. P. et al. Crowdsourcing a High-Risk Classifier for Multiple Myeloma Patients. *Blood* **130**, 265 (2017).